Microporous and Mesoporous Materials 118 (2009) 11–20

Contents lists available at ScienceDirect

Microporous and Mesoporous Materials

journal homepage: www.elsevier.com/locate/micromeso

Liquid-phase thiophene adsorption on MCM-22 zeolites. Acidity, adsorption behaviour and nature of the adsorbed products

C. Delitala [a], E. Cadoni [b], D. Delpiano [b], D. Meloni [b], M.D. Alba [c], A.I. Becerro [c], I. Ferino [b,*]

[a] Saras Ricerche e Tecnologie SpA, V strada, trav. C, Z.I. Macchiareddu, 09032 Assemini, Italy
[b] Università di Cagliari, Dipartimento di Scienze Chimiche, Complesso Universitario di Monserrato, s.s. 554 bivio sestu, 09042 Monserrato, Italy
[c] Instituto de Ciencia de Materiales de Sevilla, Departamento de Química Inorgánica (CSIC-US); Avda. Américo Vespucio 49, 41092 Sevilla, Spain

ARTICLE INFO

Article history:
Received 3 July 2008
Received in revised form 31 July 2008
Accepted 3 August 2008
Available online 12 August 2008

Keywords:
Thiophene
Adsorption
MCM-22
Calorimetry
Acidity

ABSTRACT

The liquid-phase adsorption of thiophene from thiophene/*iso*-octane solutions has been investigated in batch conditions at room temperature and atmospheric pressure on MCM-22 zeolites with Si/Al in the 9–46 range. Thiophene adsorption was found to occur in two steps whatever the Si/Al ratio of the adsorbent. The presence of ferrierite besides the MCM-22 phase caused a significant loss of the adsorption performance. For pure MCM-22 samples, the Si/Al ratio influenced the adsorption performance. Based on the acid properties of the samples, investigated by adsorption microcalorimetry of ammonia, the adsorption features were interpreted by assuming that positively charged species were originated during the first step; these species underwent successive reaction with weakly adsorbed species formed in the second step, leading to heavy molecular weight organosulphur compounds. Direct evidence for the occurrence of reactive adsorption of thiophene involving its transformation into heavy molecular weight organosulphur compounds was obtained by GC/MS investigation of the nature of the adsorbed material recovered after the adsorption experiments. The peculiar structure of MCM-22 zeolites made possible the formation of long-sized organosulphur compounds. Due to the mechanism by which thiophene is transformed (i.e. progressive addition of other thiophene molecules), the size of the resulting products was found to depend also on the concentration of the weakly adsorbed thiophene molecules able to interact with those already activated through protonation.

1. Introduction

The stringent regulations on the sulphur content of fuels and the need of ultra clean fuels for on-board and on-site reforming as sources of hydrogen for fuel cell systems make adsorption technology worthy of investigation as a route towards the deep desulphurisation of light cracked naphtha (LCN) streams, typically the major source of gasoline. The use of adsorbents for the removal of diverse sulphur compounds from various streams is documented in both the patent [1–7] and open literature [8–11]. Claims concerning the separation of thiophenic compounds from gasoline by adsorption on zeolites are reported in several patents [12–17] and some papers have also been published on the use of zeolites for the adsorption of thiophene from thiophene/hydrocarbon solutions [18–20]. Very recently, a paper dealing for the first time with the use of MCM-22 zeolite for the liquid-phase adsorption at room temperature and atmospheric pressure of thiophene and toluene from their *iso*-octane mixtures has been published by the present authors [21]. Thiophene and toluene were regarded as model compounds for the LCN organosulphur and aromatic fractions, respectively. Compared to activated carbon, MCM-22 showed superior features in the selective adsorption of thiophene from toluene-rich thiophene/toluene/*iso*-octane mixtures simulating the composition of LCN streams. This was ascribed to the reactive nature of thiophene adsorption on this solid, induced by its acidic features and favoured by its peculiar structure. For a better understanding of the complex interplay between acidity and structure in the liquid-phase thiophene adsorption process, an investigation programme dealing with use MCM-22 zeolites differing as to the Si/Al content was started in the present authors' laboratory. In a previous paper the synthesis of MCM-22 zeolites with Si/Al ratio in the 9–46 range, as well as their structural, morphological and textural characterisation has been reported [22]. It was found that the synthesis in rotating autoclave leads to a pure MCM-22 phase in the case of Si/Al = 21, 30 and 46, whereas for Si/Al = 9 a ferrierite phase crystallises besides MCM-22. Pure ferrierite was obtained in static autoclave with Si/Al ratio = 9. All the samples showed the typical texture of microporous solids. For the best crystallised samples (those with Si/Al = 21 and 30) the supermicropore to ultramicropore volume ratio was found to reflect the supercages to sinusoidal channels volume ratio in the ideal MCM-22 crystal. A variety of

* Corresponding author. Tel.: +39 070 6754383; fax: +39 070 6754388.
E-mail address: ferino@unica.it (I. Ferino).

1387-1811/$ - see front matter © 2008 Elsevier Inc. All rights reserved.
doi:10.1016/j.micromeso.2008.08.008

species were revealed on the MCM-22 samples. These include: terminal silanol groups at the external surface and internal silanol groups at open Si–O–Si linkages; OH groups associated with non-framework aluminium as well as OH groups associated with framework Al in a low condensation state; acidic OH groups of the bridging type Si(OH)Al; residual ammonium ions; basic superficial OH groups attached to extraframework Al.

In the present paper the liquid-phase thiophene adsorption on the above-cited MCM-22 samples has been dealt with. The acid properties of the samples have been also investigated by ammonia adsorption microcalorimetry; by GC/MS analysis of the organic matter recovered after the adsorption experiments, the chemical nature of the adsorbed organosulphur compounds was investigated as well. The results have been discussed in the light of the structural and textural characterisation data previously obtained [22], which are also summarized here for the sake of clarity. An interpretation of the adsorption behaviour is proposed.

2. Experimental

2.1. Materials

Hydrothermal synthesis of MCM-22 samples with Si/Al = 9, 21, 30 and 46 was carried out by using hexamethyleneimine (HMI, 99%, Aldrich) as organic template, SiO_2 (Aerosil 200, Degussa), $NaAlO_2$ (56% Al_2O_3, 37% Na_2O, Carlo Erba), NaOH (98%, Prolabo) and deionised water. Rotating autoclaves were used for the synthesis. The hydrogen forms of the MCM-22 samples were obtained by exchanging the sodium forms resulting from the synthesis with 1 M NH_4NO_3 (Carlo Erba *pro-analisi*) solution (1 h stirring at 353 K) followed by calcination in static air (overnight at 773 K). A summary of the structural and textural features of the samples is given in Table 1. Further details can be found in [22].

Table 1
Structural and textural data for the MCM-22 samples

	Si/Al = 9	Si/Al = 21	Si/Al = 30	Si/Al = 46
Crystal phase	MCM22 + Ferrierite	MCM-22	MCM-22	MCM-22
S_{DR}[a] (m^2/g)	498	597	429	356
v_{DR}[b] (cm^3/g)	0.1770	0.2121	0.1524	0.1268

[a] Surface area determined by the Dubinin–Raduskevitch method.
[b] Total micropore volume determined by the Dubinin–Raduskevitch method.

Table 2
^{1}H chemical shift, area under the curve and assignation of each curve obtained from the deconvolution of the experimental ^{1}H MAS-NMR spectra of the dehydrated MCM-22 samples [2]

Si/Al	δ (ppm)	%	Assignation
9	−4.38	13.32	basic $Al^{NF}OH$ (e)
	1.23	17.69	SiOH (a)
	1.77	2.16	SiOH (a)
	3.58	13.69	$Al^{NF}OH + Al^F$ in q^2 and q^3 (b)
	4.97	32.01	Si(OH)Al (c)
	5.82	21.05	Si(OH)Al (c)
	9.03	0.09	NH_4^+ (d)
21	−3.61	24.82	basic $Al^{NF}OH$ (e)
	1.06	13.04	SiOH (a)
	1.74	3.07	SiOH (a)
	3.43	13.08	$Al^{NF}OH + Al^F$ in q^2 and q^3 (b)
	4.90	17.82	Si(OH)Al (c)
	5.65	28.06	Si(OH)Al (c)
	9.03	0.12	NH_4^+ (d)
30	−4.68	19.15	basic $Al^{NF}OH$ (e)
	0.83	17.12	SiOH (a)
	1.72	2.34	SiOH (a)
	3.23	12.62	$Al^{NF}OH + Al^F$ in q^2 and q^3 (b)
	4.56	14.07	Si(OH)Al (c)
	5.74	34.23	Si(OH)Al (c)
	9.03	0.11	NH_4^+ (d)
46	−7.95	1.9	basic $Al^{NF}OH$ (e)
	0.3	31.16	SiOH (a)
	1.77	1.00	SiOH (a)
	3.36	14.89	$Al^{NF}OH + Al^F$ in q^2 and q^3 (b)
	5.33	33.77	Si(OH)Al (c)
	5.75	16.46	Si(OH)Al (c)
	9.17	0.81	NH_4^+ (d)

Al^{NF}: non-framework aluminium; Al^F: framework aluminium; q^2: q^2(2OSi, 2OH) aluminium environments; q^3: q^3(3OSi, 1OH) aluminium environments. Letters within brackets refer to the code used in the text.

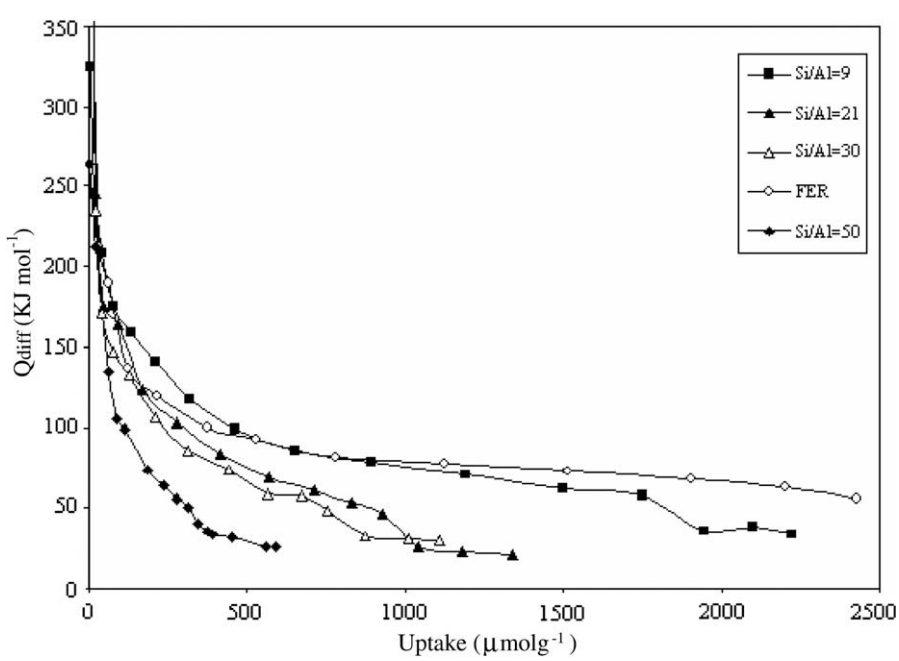

Fig. 1. Differential heat of adsorption, Q_{diff}, as a function of ammonia uptake, n_A, for the MCM-22 samples. The curve for the pure ferrierite sample is also reported for completeness.

2.2. Surface acidity assessment

Surface acidity was investigated by adsorption microcalorimetry on a Tian-Calvet heat flow equipment (C80, Setaram) using ammonia as a probe molecule. Each sample was pre-treated overnight at 673 K under vacuum (10^{-3} Pa) before the successive introduction of small doses of ammonia at 353 K. Procedural and instrumentation details can be found in [21]. The adsorption and calorimetric isotherms were obtained for each adsorption/readsorption experiment. The overall uptake of the probe gas on the solid was assessed from the first isotherm; the amount of ammonia irreversibly adsorbed was calculated by subtracting from the first isotherm the second one, obtained after outgassing the sample. Details on the data treatment can be found elsewhere [23].

2.3. Adsorption experiments

Adsorption experiments were carried out in batch conditions at room temperature and atmospheric pressure in a modified FC6S Jar Test apparatus (Velp Scientifica). Thiophene was supplied by Fluka (*purum* grade). Prior to the adsorption runs, the MCM-22 samples were heated in flowing air (3 K min^{-1} up to 473 K, hold 1 h,

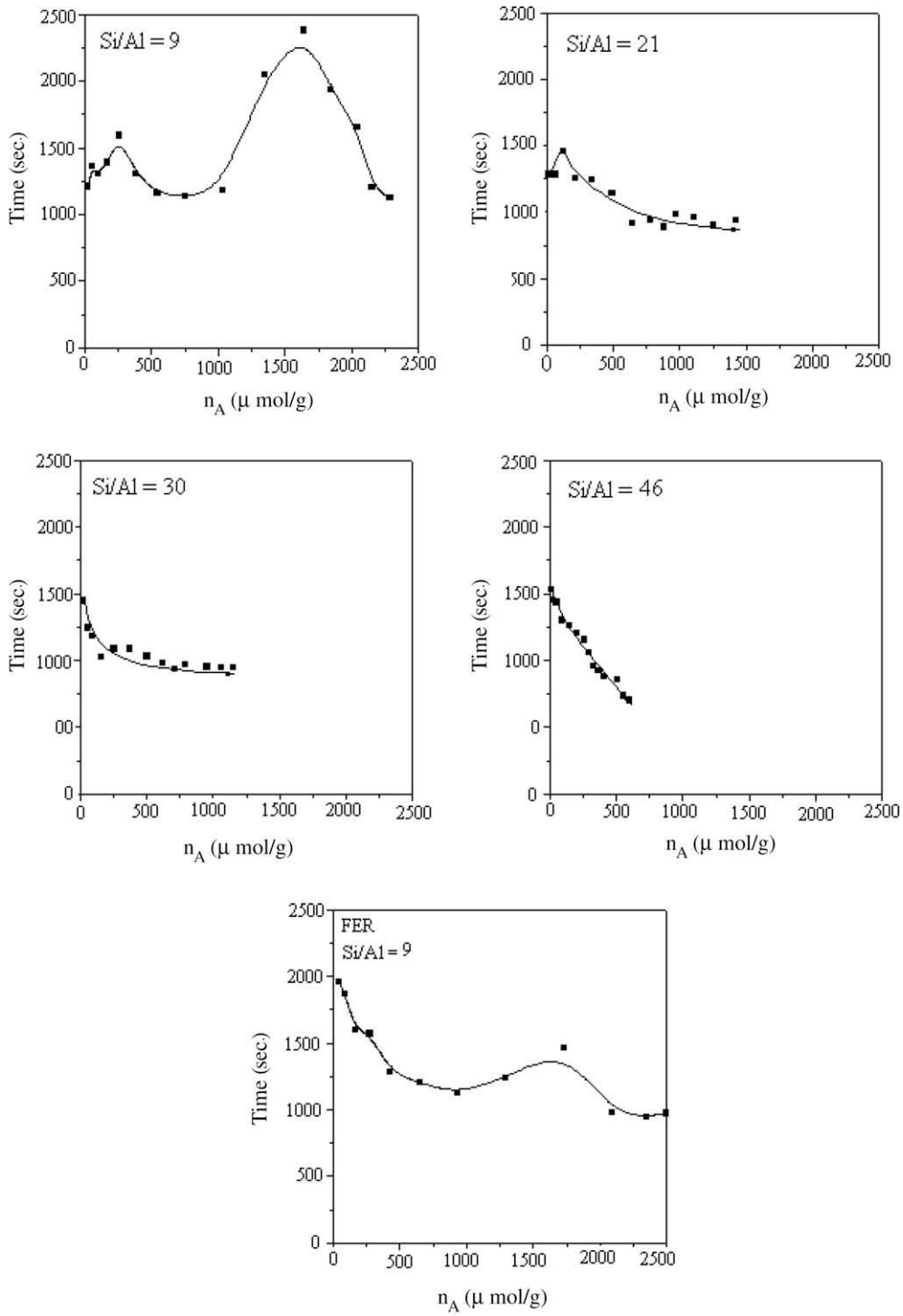

Fig. 2. Thermokinetic parameter, t_o, vs. ammonia uptake for the MCM-22 and ferrierite samples.

1 K min^{-1} up to 723 K, hold 12 h). The thiophene content in the thiophene/*iso*-octane solution was determined by HPLC before and after each experiment; the initial concentration for thiophene was varied in the range 4.33×10^{-5} to 2.43×10^{-2} mol L^{-1}. The HPLC apparatus (Agilent Technologies, 1100 series) was equipped with a Lichrospher 100 NH_2 250 × 4 mm ID, 5 μm column, and UV and Refractive Index detectors; *n*-heptane was used as eluent. Further details can be found in [21].

2.4. Recovery and analysis of the adsorbed products

A method first reported [24] for the characterisation of coke retained on zeolites during acid-catalysed reactions was used. After the adsorption experiment, the adsorbent was separated from the thiophene/*iso*-octane mixture by filtration and treated with a 40% hydrofluoric acid solution, followed by extraction of the organic compounds by methylene chloride. The solvent was then evaporated and an oily liquid recovered, which was analysed by GC/MS. Details can be found in [21].

3. Results and discussion

3.1. Adsorption calorimetry

Ammonia was chosen as a probe molecule in calorimetric runs aimed at assessing the surface acidity of the MCM-22 samples, which is expected to influence their adsorption features, due to the basic character of tiophene. The results are summarized in Fig. 1, where the differential heat of adsorption, Q_{diff}, is plotted vs. the ammonia uptake, n_A.

The latter is expressed on a per mass unit basis, instead of a per surface area unit basis, so that direct comparison with thiophene adsorption data, also given on a per mass unit basis (cf. Section 3.2), can be carried out, as will be shown later on. For all the MCM-22 samples Q_{diff} decreases from 245-210 to ca. 25 kJ mol^{-1} as the coverage increases, until a total ammonia uptake ranging from ca. 580 to ca. 2225 μmol g^{-1} is attained. The calculated (cf. Section 2) amounts of ammonia irreversibly adsorbed were 1020, 560, 460 and 170 μmol g^{-1}, for the samples with Si/Al = 9, 21, 30 and 46, respectively. Roughly three regions can be individuated

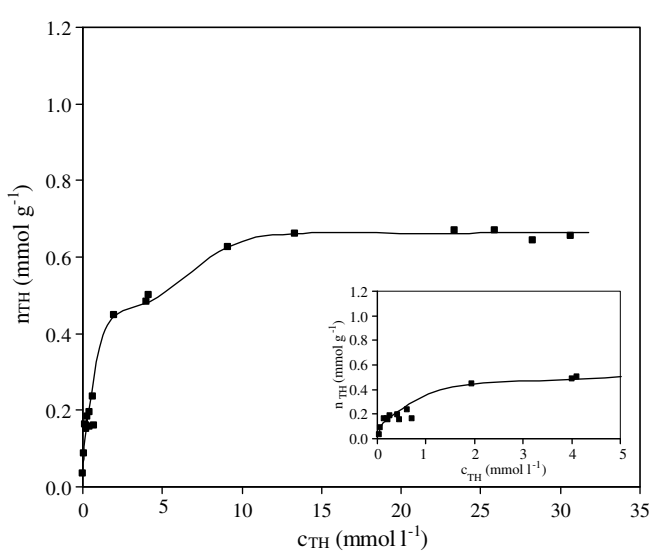

Fig. 3. Isotherm for thiophene adsorption on the MCM-22 sample with Si/Al = 9. c_{TH} and n_{TH} represent the equilibrium concentration of thiophene in the liquid phase and the thiophene adsorbed amount, respectively. Details on the first adsorption region are shown in the inset.

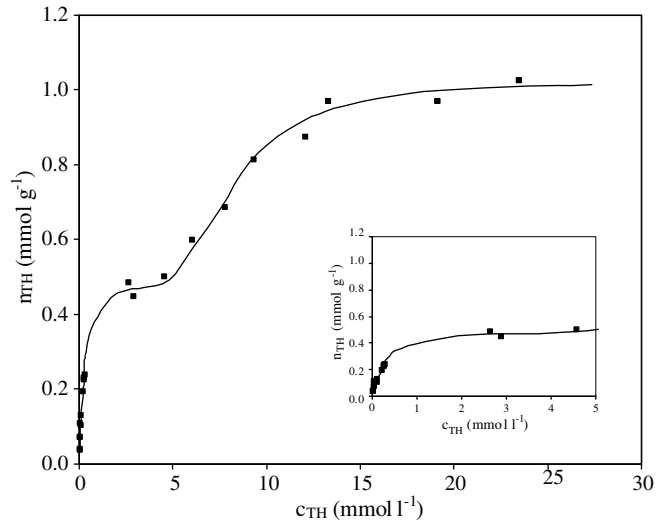

Fig. 4. Isotherm for thiophene adsorption on the MCM-22 sample with Si/Al = 21. c_{TH}, n_{TH} and inset as in Fig. 3.

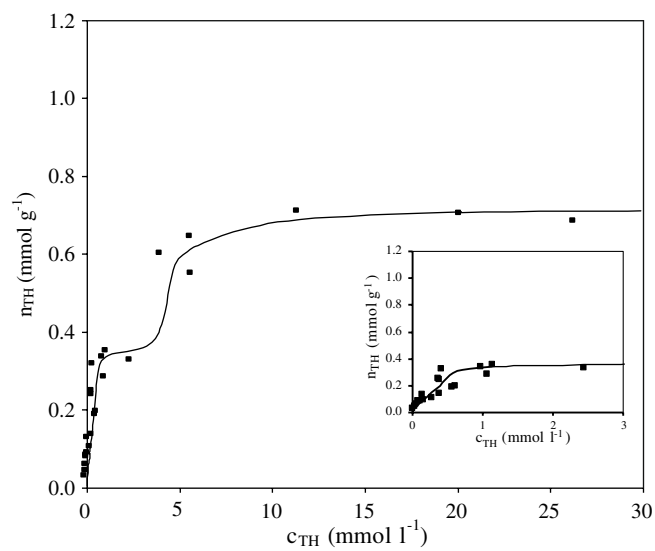

Fig. 5. Isotherm for thiophene adsorption on the MCM-22 sample with Si/Al = 30. c_{TH}, n_{TH} and inset as in Fig. 3.

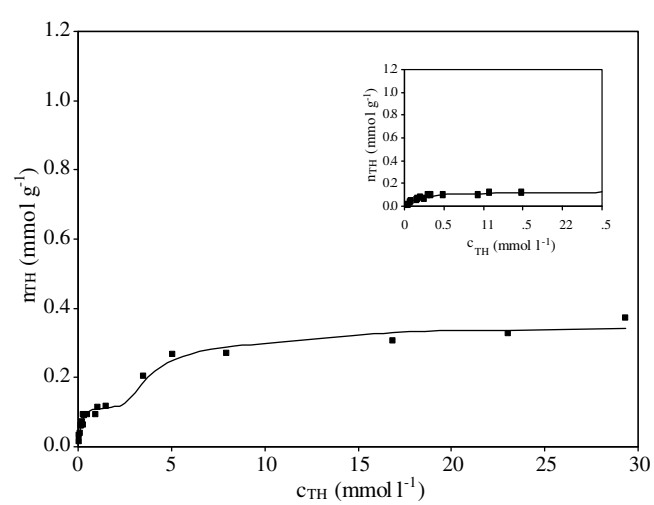

Fig. 6. Isotherm for thiophene adsorption on the MCM-22 sample with Si/Al = 46. c_{TH}, n_{TH} and inset as in Fig. 3.

in the Q_{diff} vs. n_A profile of each sample: (i) a marked decrease from 245-210 to ca. 70 kJ mol^{-1}, as n_A approaches the completion of irreversible adsorption; (ii) a smoother decrease to ca. 50 kJ mol^{-1}, attained at n_A values of ≅1755, 980, 765 and 315 μmol g^{-1} for the samples with Si/Al = 9, 21, 30 and 46, respectively; (iii) a stepwise drop to ca. 25 kJ mol^{-1}, which value remains roughly constant until the end of the uptake process.

Such low values of Q_{diff} as those of region (iii) are so close to the liquefaction heat of ammonia (20.2 kJ mol^{-1} at 353 K, calculated by the Watson relation [25]) that the corresponding ammonia uptake cannot be ascribed to interactions with surface sites; rather, it would be related to condensation-like phenomena occurring on the solid surface.

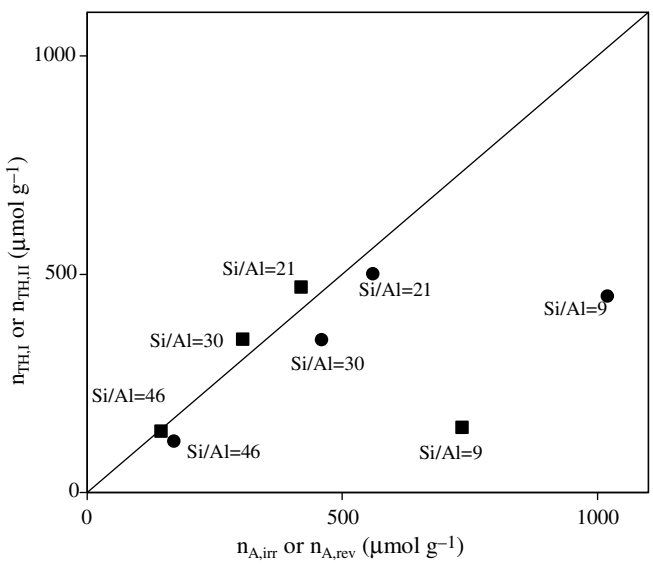

Fig. 7. Amount of thiophene adsorbed on the MCM-22 samples during the first step, $n_{TH,I}$, as a function of the concentration of the acid sites able to adsorb ammonia irreversibly, $n_{A,irr}$ (●) and amount of thiophene adsorbed during the second step, $n_{TH,II}$, as a function of the concentration of the acid sites able to adsorb ammonia reversibly, $n_{A,rev}$ (■).

The Q_{diff} values of region (ii) lie in a narrow range (70–50 kJ mol^{-1}) and are originated by reversible adsorption of ammonia. In a previous paper from this laboratory [21], it was assumed that the sites responsible for such weak adsorption on an MCM-22 sample were silanol groups; this was done because differential adsorption heats ranging from ca. 70 to ca. 50 kJ mol^{-1} had been previously measured in ammonia adsorption experiments on pure silica samples [26,27]. Based on the NMR results reported in [22] for the present MCM-22 samples it appears, however, that the assumption that silanols are the only sites responsible for the weak adsorption of ammonia in region (ii) is oversimplified, as shown below. The results of the NMR analysis carried out in [22] are summarized in Table 2. From the assignments there reported it should be concluded that ammonia adsorption cannot occur on type (e) species, due to their basic character; neither can it take place on type (d) species, i.e. ammonium ions. The species able to interact with ammonia should be those of type (a) (i.e. silanols), type (b) (i.e. OH groups associated with non-framework aluminium as well as OH groups associated with framework Al in a low condensation state) and type (c) (i.e. bridging Si(OH)Al species). Their amounts are indicated in Table 2 by the corresponding % area. The fraction of type (a) species (i.e. silanols) over the total (a) + (b) + (c) species (i.e. those able to adsorb ammonia) can be easily calculated, giving 23%, 21%, 25% and 33% for the samples with Si/Al = 9, 21, 30 and 46, respectively. From the calorimetric data the sites adsorbing ammonia with differential heats in the 70–50 kJ mol^{-1} account for 42%, 43%, 40% and 46% of the total ammonia-adsorbing sites, which clearly indicates that the reversible ammonia adsorption cannot be ascribed to silanols only. It is worthy of note, however, that the above calorimetric data nicely match with the fraction of (a) + (b) species over the total (a) + (b) + (c) species (39%, 39%, 41% and 48%, for the samples with Si/Al = 9, 21, 30 and 46, respectively). Accordingly, the weak adsorption corresponding to region (ii) (differential heats in the 70–50 range) is originated by the

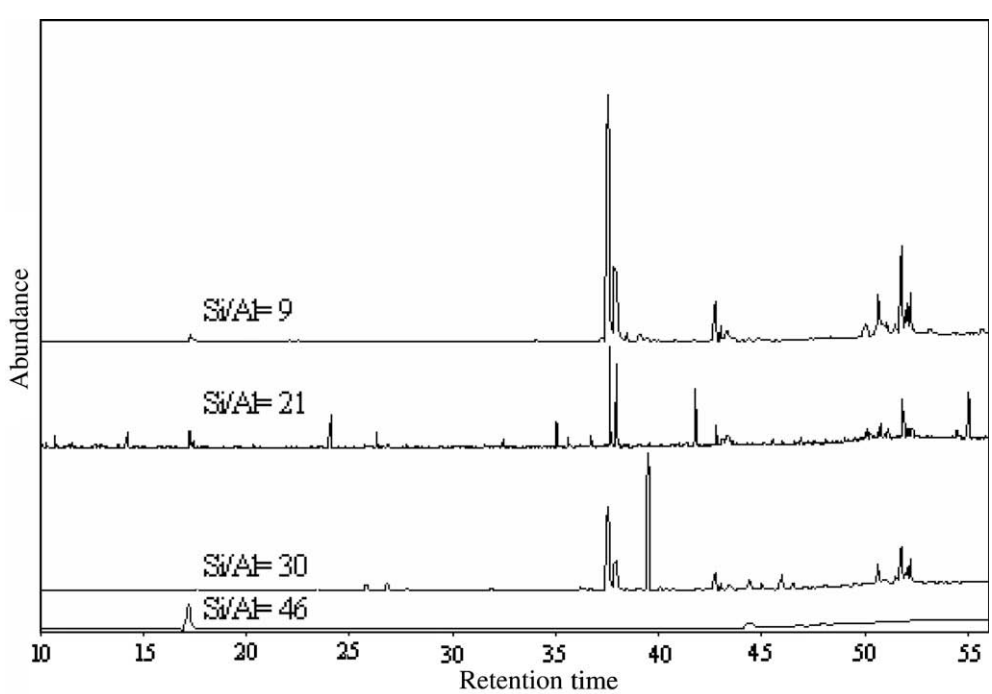

Fig. 8. TIC signals of compounds retained by MCM-22 samples after thiophene adsorption from thiophene/*iso*-octane mixtures. (Experimental conditions as for the last point in Figs. 3–6.)

interaction of ammonia not only with silanols, but also with OH groups associated with non-framework aluminium and OH groups associated with framework Al in a low condensation state, q^3(3OSi, 1OH) and q^2(2OSi, 2OH).

The irreversible adsorption corresponding to region (i) would be originated by the interaction of ammonia with the remarkably acidic Si(OH)Al species. The decreasing trend of Q_{diff} in this region is indicative of heterogeneity in the strength of these ammonia-

Table 3
Main compounds revealed by GC/MS analysis of the material retained by MCM-22 samples after thiophene adsorption from thiophene/*iso*-octane solution

Code	Retention time	Molecular weight	Structure	Abundance (%)		
				Si/Al = 9	Si/Al = 21	Si/Al = 30
1	37.62;37.96	252	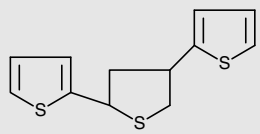 (2 diastereoisomers) ($C_{12}H_{12}S_3$)	54.6	32.3	29.8
2	[50.11–52.31]	336	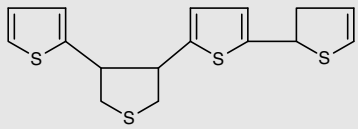 (Family of isomers and/or diastereoisomers) ($C_{16}H_{16}S_4$)	34.3	25.1	32.0
3	42.83	302	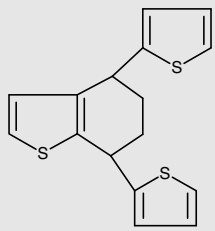 ($C_{16}H_{14}S_3$)	7.5	3.9	5.3
4	24.06	208	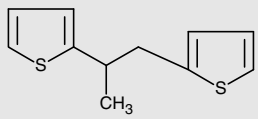 ($C_{11}H_{12}S_2$)	nd	4.8	nd
5	41.76	332	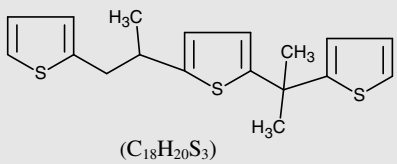 ($C_{18}H_{20}S_3$)	nd	10.6	nd
6	55.05	456	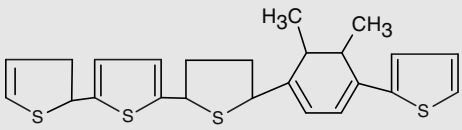 ($C_{25}H_{27}S_4$)	nd	15.2	nd
7	39.47	304	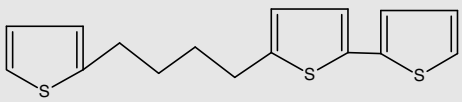 ($C_{16}H_{16}S_3$)	nd	nd	20.0

adsorbing sites. Such heterogeneity stems from the different nature and location of the acid sites in the MCM-22 samples, already evidenced by the NMR results [22]. For the Si/Al = 9 sample an additional factor causing heterogeneity in the acid strength is the simultaneous presence of two zeolithic phases, namely MCM-22 and ferrierite. (The Q_{diff} vs. ammonia uptake curve for the pure ferrierite sample is also reported in Fig. 1 for completeness.)

Additional insight into the ammonia adsorption process can be obtained by considering thermokinetic data. The time over which the heat is evolved after each successive dose (thermokinetic parameter, t_o) is plotted in Fig. 2 vs. the ammonia uptake for all the samples, pure ferrierite included. Interestingly, the t_o vs. n_A plot shows a maximum for ferrierite and two maxima for the Si/Al = 9 sample, the second maximum of the latter being remarkably high. No maxima are visible for the pure MCM-22 samples (i.e. with Si/Al = 21, 30 and 46). The presence of maxima in the t_o vs. coverage plots is considered [26] to indicate that surface diffusion is the mechanism by which the sites are selectively titrated during sequential exposure to the probe molecules. At low coverage, the probe is adsorbed on the strong sites, where it remains irreversibly held, giving a low thermokinetic parameter. As coverage increases, the number of strong sites still available decreases and a competition between strong and weak sites takes place for the adsorption of the probe molecules. Those by chance adsorbed on the weak sites are able to migrate to the stronger sites; the smaller the number of strong sites, the slower this surface equilibration process (as the molecules must diffuse over greater distances) and hence the thermokinetic parameter increases. The lack of maxima for the pure MCM-22 samples hence suggests that ammonia diffusion occurs very fast in the pore system of these samples. By converse, the maximum observed for ferrierite in the region of reversible ammonia uptake suggests that the titration of the corresponding sites is governed by the slow surface diffusion of the probe. This is consistent with the pore structure of ferrierite, characterised by a two-dimensional channel system with pores of 10 MR (0.42×0.54 nm) and 8 MR (0.35×0.48 nm), i.e. somewhat constrained in comparison with that of MCM-22. The latter has a framework in which 10 MR openings give access to two independent pore systems: a tridimensional one, formed by large cylindrical supercages ($0.71 \times 0.71 \times 1.84$ nm) interconnected by straight and oblique (0.40×0.55 nm) channels, and a bidimensional one, formed by interconnected sinusoidal channels (0.40×0.50 nm) surrounding the double 6-member ring connecting the supercages. Such restrictions in the surface mobility of ammonia as those observed for ferrierite also operate on the MCM-22 sample with Si/Al = 9, which actually contains a ferrierite phase. The presence of the latter also causes the surface diffusion of ammonia to slowdown during the strong sites titration, as suggested by the peak in the irreversible region of uptake.

3.2. Thiophene adsorption runs

Adsorption equilibrium data were obtained by contacting the MCM-22 samples with thiophene/*iso*-octane mixtures. The corresponding adsorption isotherms, covering a wide range of thiophene concentration in the thiophene/*iso*-octane mixtures, are reported in Figs. 3–6. All the samples are able to separate thiophene from thiophene/*iso*-octane solutions, though to a different extent. Their performance as adsorbents is influenced by the purity extent of the MCM-22 phase, and, for the pure MCM-22 samples, by the Si/Al ratio: the higher its value, the better the performance. A common feature to all the isotherms is their stepwise character: the thiophene adsorbed amount, n_{TH}, increases along with the equilibrium concentration of thiophene in the liquid phase, c_{TH}, until a short plateau is attained; a second, wide plateau is then attained as c_{TH} further increases. Such a behaviour, indicating (partial or complete) saturation of thiophene-adsorbing sites of some kind followed by a second adsorption step on surface sites of a different kind, had been previously found [21] to be typical of thiophene, which at variance from toluene, underwent reactive adsorption on an MCM-22 sample. The first adsorption step was there ascribed to the interaction of thiophene with the acid sites, whereas the second adsorption step was assumed to stem from the interaction of further thiophene molecules from the liquid phase with the weaker surface sites.

The present results (Figs. 3–6) can be used to check whether the above outlined behaviour represents a general feature of MCM-22 zeolites, i.e. it is typical of this structure whatever the Si/Al ratio. With this aim, the amount of thiophene corresponding to the first saturation step, $n_{TH,I}$, has been plotted in Fig. 7 vs. the concentration of the acid sites able to adsorb ammonia irreversibly, n_{irr} (from the calorimetric data, Section 3.1). In the same Fig. 7, the thiophene amount adsorbed during the second step, $n_{TH,II}$, calculated as the difference between the n_{TH} values of the higher and lower plateaus in Figs. 3–6, has been plotted vs. the concentration of the acid sites able to adsorb ammonia reversibly, n_{rev}. For the MCM-22 samples with Si/Al = 21, 30 and 46 a fair correlation is observed between $n_{TH,I}$ and n_{irr}, on the one hand, and between $n_{TH,II}$ and n_{rev}, on the other. The correlation does not hold for the Si/Al = 9 sample, for which the amount of thiophene adsorbed during the first and sec-

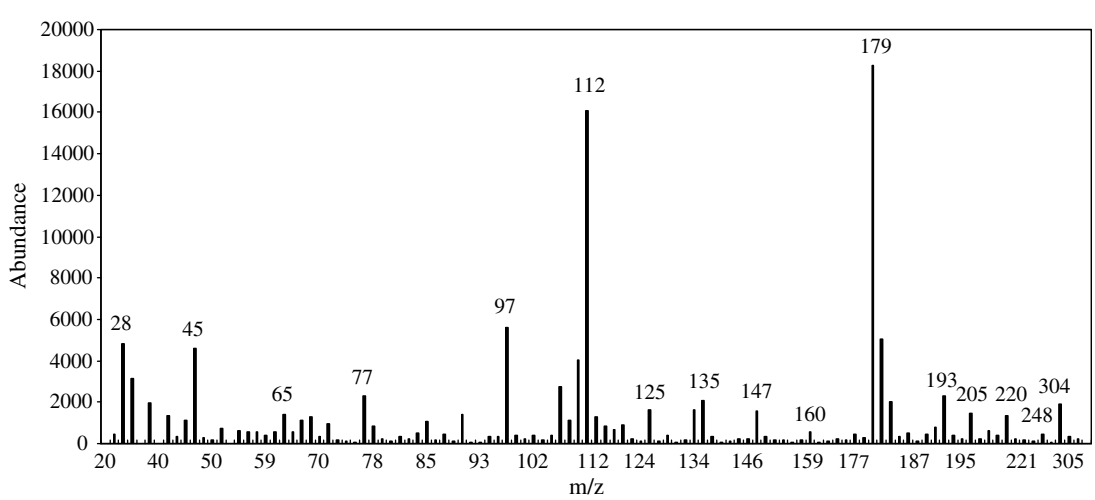

Fig. 9. Mass spectrum corresponding to the peak at r.t. 39.47 min. in the TIC signal for the Si/Al = 30 sample.

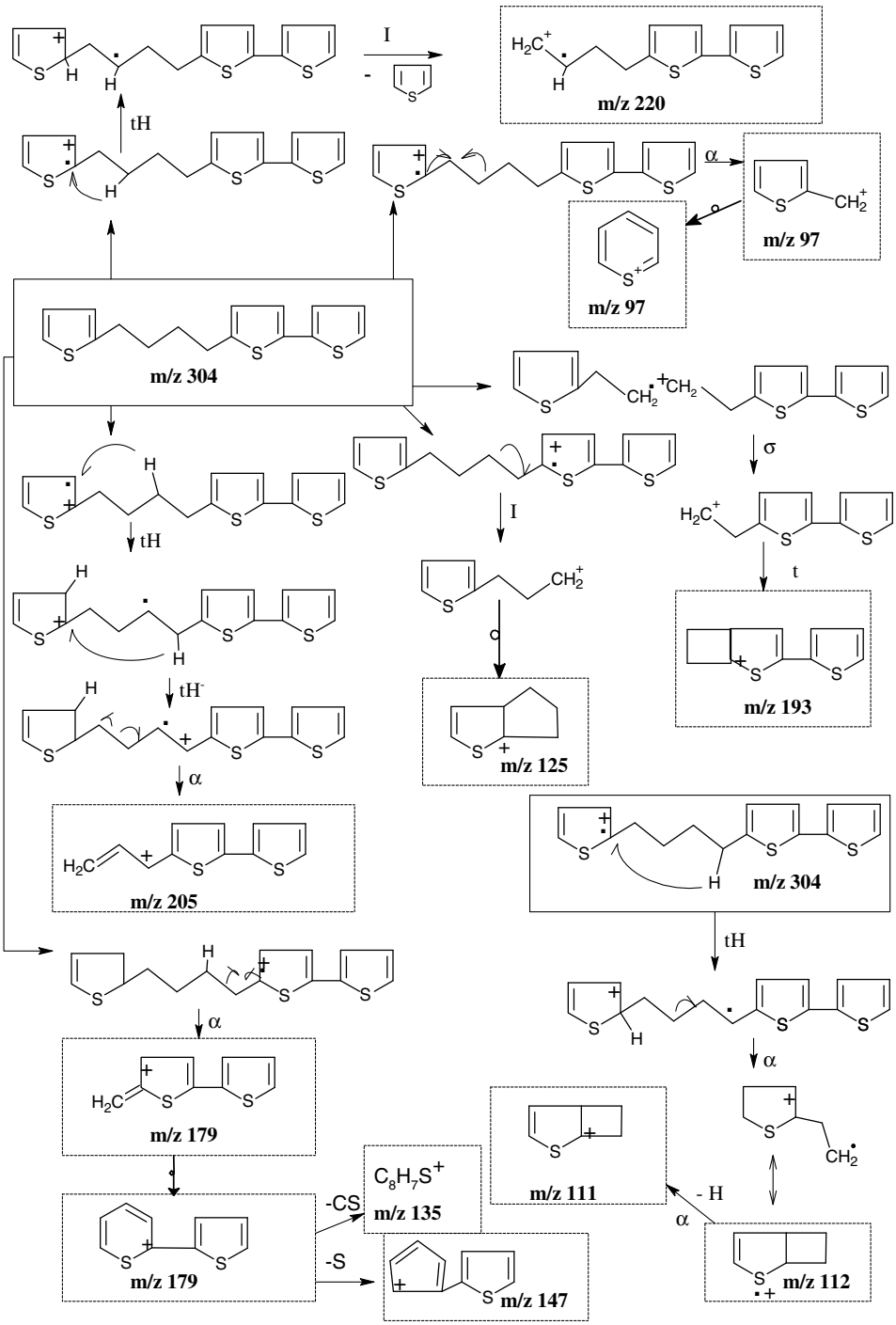

Scheme 1.

ond step is much lower than expected on the basis of its concentration of strong (i.e. irreversibly adsorbing ammonia) and weak (i.e. reversibly adsorbing ammonia) sites, respectively. In the light of the diffusional limitations revealed by the thermokinetic data for ammonia adsorption (cf. Section 3.1), the poor performance (in spite of its acidic features) of MCM-22 with Si/Al = 9 can be ascribed to the hindered access of thiophene to the acid sites, induced by the presence of the ferrierite phase. Indeed, pure ferrierite (synthesised under static conditions from a gel of the same composition of that which led to the MCM-22 sample with Si/Al = 9) showed no ability to adsorb thiophene when contacted with thiophene/*iso*-octane solutions. It is also worthy of note that for the MCM-22 sample with Si/Al = 9 the amount of thiophene adsorbed during the second step appears much more underestimated than the amount adsorbed during the first step (Fig. 7). This is in agreement with the finding that surface diffusion constraints concern much more the access to the sites able to adsorb ammonia reversibly rather than the access to the sites able to adsorb ammonia irreversibly (in Fig. 2 the maximum for t_o in the reversible range of uptake is much larger than the one in the irreversible range).

3.3. Chemical nature of the adsorbed products

The colour taken by the samples during the adsorption runs is worthy of note. A shortwhile after contacting the Si/Al = 9, 21, 30

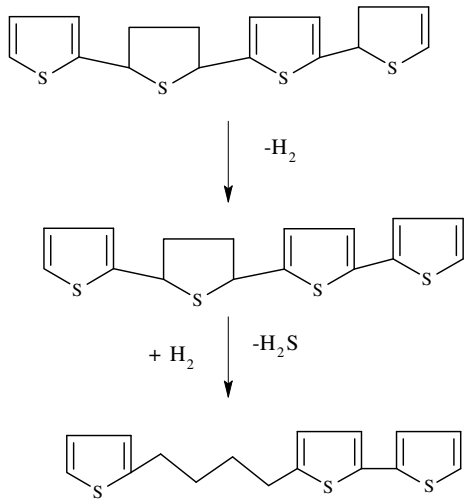

Scheme 2.

and 46 zeolites with the thiophene/*iso*-octane solution, their original white colour changed to orange, deep, pale and very pale yellow, respectively. Orange-yellow coloured species were reported to form upon gas-phase adsorption of thiophene on HY zeolites also by other authors [28], who identified them as oligomeric species by spectroscopic techniques. The colour intensity, which is obviously related to the amount of the oligomer species, progressively fades for the present samples along with the progressive decrease of the concentration of the acid sites and the amount of thiophene adsorbed. It can be reasonably assumed that oligomerisation reactions are initiated by thiophene protonation, occurring by interaction with the acidic sites of MCM-22 during the first adsorption step. The second adsorption step, originated by interaction of further thiophene molecules from the liquid phase with weaker surface sites, would cause an increase in the local concentration of thiophene in the confined environment of the MCM-22 supercages. Due to the close proximity of the already formed protonated thiophene molecules, bimolecular oligomerisation reactions would occur.

To check the occurrence of such reactions on the present MCM-22 samples, GC/MS analysis of the organosulphur compounds retained by the adsorbents after the adsorption experiments has been carried out. The TIC signals for all the MCM-22 samples are shown in Fig. 8. On the basis of the mass spectra, the peaks in Fig. 8 have been assigned to the products listed in Table 3. Formation of 1, 2 and 3 products is a common feature of the MCM-22 zeolites with Si/Al = 9, 21 and 30. Besides these compounds, heavier compounds 4, 5 and 6 also form on MCM-22 with Si/Al = 21, as already reported in [21], where the relevant mass spectra and a detailed description of the fragmentation pathways for 1–6 compounds can be found, as well as an outline of the the complex reactions leading to their formation. Product 7 (whose mass spectrum and fragmentation pathway are shown in Fig. 9 and Scheme 1, respectively) forms on the Si/Al = 30 sample, where compounds 1, 2 and 3 (and traces of 4, 5, 6) form as well. The formation of product 7 can be traced back to the transformation of family 2 compounds through dehydrogenation followed by desulphuration (Scheme 2). None of the products in Table 3 was revealed for the MCM-22 sample with Si/Al = 46. For the latter, the amount of the adsorbed material was probably too small for allowing significant recovery in methylene chloride after the adsorption experiments; this is also in agreement with the very pale yellow colour taken by this sample after contacting it with the thiophene/*iso*-octane solution.

It is manifest from the above that thiophene adsorption on the MCM-22 samples, with the exception of the one with Si/Al = 46, for which the data are not conclusive, involves its transformation into heavy molecular weight organosulphur compounds. The peculiar structure of MCM-22 zeolites makes possible the formation of such a long-sized compound as 6 (1.98×0.71 nm), which could not form on other zeolites. Thus, in the organosulphur material retained by H–Y zeolite after liquid-phase thiophene adsorption only product 1 and compounds similar to 2 and 3 have been detected [20]. This does not mean however that the formation of long-sized compounds invariably occurs whenever an MCM-22 sample is used as a thiophene adsorbent. Due to the mechanism by which thiophene is transformed (i.e. progressive addition of other thiophene molecules), the size of the resulting products would depend also on the concentration of the weakly adsorbed thiophene molecules able to interact with those already activated through protonation. This would explain why, despite the favourable structural features, the largest (and most abundant) product formed on the MCM-22 with Si/Al = 30 is 7 (1.69×0.41 nm), whereas only traces of product 6 (1.98×0.71 nm) are detected: the amount of thiophene weakly adsorbed is not high enough for allowing the growth of the organosulphur compounds to such a size. Though the acid features of the sample with Si/Al = 9 are similar to those of the sample with Si/Al = 30, the presence in the former of ferrierite hinders a comparison between them. It is worthy of note however that the products formed on the Si/Al = 9 are the same of (or similar to) those reported for H–Y [20].

4. Conclusions

The following conclusions can be drawn. (i) MCM-22 zeolites are able to separate thiophene from thiophene/*iso*-octane solutions, whatever their Si/Al ratio in the range 9–46, the most promising sample for sulphur removal being the one with Si/Al = 21. (ii) Significant loss of the adsorption performance occurs when a ferrierite phase is present in the adsorbent besides MCM-22; it seems that the former hinders, to some extent, the access of thiophene to the MCM-22 pore system. (iii) For pure MCM-22, the Si/Al ratio influences the adsorption performance, in that it determines the acidic features of each sample. (iv) A common feature to all the MCM-22 samples is that the thiophene adsorption occurs in two steps; it seems that adsorption occurs first on strong acid sites (measured as those able to adsorb ammonia irreversibly and identified as Si(OH)Al species) and then continues on weak sites (measured as those able to adsorb ammonia reversibly and identified as silanols, OH groups associated with non-framework aluminium and OH groups associated with framework Al in a low condensation state). (v) Positively charged species originated during the first step undergo reaction with weakly adsorbed species formed in the second step, leading to heavy molecular weight organosulphur compounds.

Acknowledgments

Financial support from the Project funded within the VI Framework Programme as an HRM Activity under contract number MRTN-CT-2006-035957, DGICYT Project No. CTQ2007-63297 and the Excellence Project from Junta de Andalucía P06-FQM-02179 is gratefully acknowledged.

References

[1] P.E. Eberly, W.E. Winter (Exxon Research and Engineering Co.), US Patent 4,464,252 (1984).
[2] G.C. Allen (El Paso Products Co.), US Patent 4,540,842 (1985).
[3] M.M. Nagij, E.S. Holmes, J.L. Pai (UOP), US Patent 5,114,689 (1992).
[4] G.W. Dodwell (Phillips Petroleum Co.), US Patent 6,429,170 (2002).
[5] R.P. Gupta, B.S. Turk (Research Triangle Institute), International Patent WO 02/22763A1 (2002).

[6] M.A. Poirier (Exxon Research and Engineering Co.), US Patent 6,027,636 (2000).
[7] W. Wismann, S.K. Gangwall (DS2 Tech. Inc.), US Patent Appl. US2002/0043482 A1 (2002).
[8] A.B.S.H. Salem, H.S. Hamid, Chem. Eng. Technol. 20 (1997) 342.
[9] X. Ma, L. Sun, C. Song, Catal. Today 77 (2002) 107.
[10] S. Mikhail, T. Zaki, L. Khalil, Appl. Catal. A: Gen. 227 (2002) 265.
[11] E. Aust, B. Bruccolini, Oil Gas Eur. Mag. 2 (2004) 92.
[12] J.M. Brooke (Phillips Petroleum Co.), US Patent 3,051,646 (1962).
[13] E.L. Clark (Union Carbide Corporation), US Patent 3,211,644 (1965).
[14] P.H.T. Katonah, M.N.Y. Lee, Y. Heights, K.D. Manchanda (Union Carbide Corporation), US Patent 3,620,969 (1969).
[15] H.A. Zinnen, T.N. Laszlo, J.R. Holmgrem, B.J. Arena (UOP LLC), US Patent 5,843,300 (1998).
[16] H.A. Zinnen (UOP LLC), US Patent 5,935,422 (1999).
[17] R. Bartek (Marathon Oil Co.), US Patent 5,919,354 (1999).
[18] J. Weitkamp, M. Schwark, S. Ernst, J. Chem. Soc., Chem. Commun. (1991) 1133.
[19] A.J. Hernandez-Maldonado, R.T. Yang, Ind. Eng. Chem. Res. 42 (2003) 123.
[20] D. Richardeau, G. Joly, C. Canaff, P. Magnoux, M. Guisnet, M. Thomas, A. Nicolaos, Appl. Catal. A: Gen. 263 (2004) 49.
[21] C. Delitala, E. Cadoni, D. Delpiano, D. Meloni, S. Melis, I. Ferino, Micropor. Mesopor. Mater. 110 (2008) 197.
[22] C. Delitala, M.D. Alba, A.I. Becero, D. Delpiano, D. Meloni, I. Ferino, Micropor. Mesopor. Mater. 118 (2009) 1.
[23] M.G. Cutrufello, I. Ferino, R. Monaci, E. Rombi, V. Solinas, Top. Catal. 19 (2002) 225.
[24] M. Guisnet, P. Magnoux, Appl. Catal. 54 (1989) 1.
[25] R.C. Reid, J.M. Prausnitz, B.E. Poling, The Properties of Gases and Liquids, fourth ed., McGraw-Hill, New York, 1987.
[26] N. Cardona-Martinez, J.A. Dumesic, J. Catal. 125 (1990) 427.
[27] G. Colón, I. Ferino, E. Rombi, E. Selli, L. Forni, P. Magnoux, M. Guisnet, Appl. Catal. A: Gen. 168 (1998) 81.
[28] F. Geobaldo, G. Turnes Palomino, S. Bordiga, A. Zecchina, C. Otero Areán, Phys. Chem. Chem. Phys. 1 (1999) 561.